JOURNAL OF THERMOPHYSICS AND HEAT TRANSFER
Vol. 20, No. 4, October–December 2006

Least-Squares Collocation Meshless Approach for Transient Radiative Transfer

J. Y. Tan,* L. H. Liu,† and B. X. Li‡
Harbin Institute of Technology, 150001 Harbin, People's Republic of China

DOI: 10.2514/1.19583

A least-squares collocation meshless method based on the discrete-ordinates equation is extended to solve a transient radiative transfer problem in absorbing, emitting, and scattering media. The fully implicit scheme is used to discretize the transient term. A moving least-squares approximation is applied to construct the trial functions. In addition to the collocation points that are used to construct the trial functions, a number of auxiliary points are also added to form the total residuals of the problem. The least-squares technique is used to obtain the solution of the problem by minimizing the sum of the residuals for all collocation and auxiliary points. Three numerical examples are studied to illustrate the performance of this new solution method. The numerical results are compared with the other benchmark approximate solutions. By comparison, the results show that the least-squares collocation meshless method is efficient, accurate, and stable, and can be used for solving transient radiative transfer problems in participating media.

Nomenclature

$\mathbf{A}$	=	matrix defined in Eq. (7)
a	=	coefficients for moving least-squares (MLS) approximation in Eq. (4)
$\mathbf{a}$	=	vector of coefficient a
$\mathbf{B}$	=	matrix defined in Eq. (8)
C_j	=	expansion coefficient of scattering phase function
C^m	=	coefficient defined in Eq. (14b)
c	=	propagation speed of radiant energy, m/s
D^m	=	coefficient defined in Eq. (14a)
f	=	coefficients in linear equations
G	=	incident radiation, $\mathrm{W/m^3}$
g	=	quartic spline function defined in Eq. (20)
I	=	radiative intensity, $\mathrm{W/m^2 \cdot sr}$
$\tilde{I}$	=	MLS approximant of radiative intensity, $\mathrm{W/m^2 \cdot sr}$
$\hat{I}$	=	fictitious radiative intensity, $\mathrm{W/m^2 \cdot sr}$
$\hat{\mathbf{I}}$	=	vector of trial function defined in Eq. (9)
I_b	=	blackbody radiative intensity, $\mathrm{W/m^2 \cdot sr}$
J	=	weighted discrete L_2 norm defined in Eq. (5)
K	=	coefficients in linear equations
k	=	order of monomial basis function
L	=	medium thickness, side length of square enclosure, m
l	=	spatial coordinate, x, y, and z
M	=	number of discrete ordinates
N_{aux}	=	number of auxiliary points
N_{col}	=	number of collocation points
n	=	number of the nodes used for MLS approximation
$\mathbf{n}_w$	=	outward unit normal vector of boundary surface
P_j	=	Legendre polynomial
$\mathbf{p}$	=	monomial basis function
q_x, q_y	=	radiative heat flux in the x and y coordinate directions, $\mathrm{W/m^2}$
R_Q^m	=	residual function for the discrete-ordinates equation at the point $\mathbf{x}_Q$
r	=	dimensionless distance
S_n	=	discrete-ordinates scheme
$\mathbf{s}_m$	=	unit vector in the direction m
T	=	temperature, K
T_g	=	medium temperature, K
T_w	=	wall temperature, K
T_{w_0}	=	temperature of plate at $x = 0$, K
t	=	time, s
t^*	=	dimensionless time, $t^* = \beta ct$
$V_{\mathbf{x}}$	=	domain of definition of the MLS approximation for the trial function at $\mathbf{x}$
w^m	=	weight corresponding to the direction m
w^{MLS}	=	MLS weight function
$\mathbf{x}$	=	space position vector
x, y, z	=	Cartesian coordinates, m
α_{MLS}	=	dimensionless size parameter
β	=	extinction coefficient, $\beta = \kappa_a + \kappa_s$, $\mathrm{m^{-1}}$
Γ	=	function of all residuals for all collocation and auxiliary points
Δt	=	time step, s
Δt^*	=	dimensionless time step, $\Delta t^* = \beta c \Delta t$
Δx, Δy	=	average nodal spacing between two neighbor collocation points in x and y coordinate directions, respectively
ε_w	=	wall emissivity
κ_a	=	absorption coefficient, $\mathrm{m^{-1}}$
κ_s	=	scattering coefficient, $\mathrm{m^{-1}}$
μ, η, ξ	=	direction cosines of discrete ordinates
σ	=	Stefan–Boltzmann constant, $\mathrm{W/m^2 \cdot K^4}$
τ_x, τ_y	=	optical thickness variables, $\tau_x = \beta x$, $\tau_y = \beta y$
τ_L	=	optical thickness of plate, $\tau_L = \beta L$
Φ	=	scattering phase function
ϕ	=	shape function
ω	=	single scattering albedo, $= \kappa_s/\beta$

Subscript

w	=	value at boundary wall

Superscripts

old	=	value of the last time calculation

Received 20 August 2005; revision received 15 February 2006; accepted for publication 24 February 2006.

*Ph.D. Candidate, School of Energy Science and Engineering, 92 West Dazhi Street; tanjy@hit.edu.cn.

†Professor, School of Energy Science and Engineering, 92 West Dazhi Street; lhliu@hit.edu.cn (corresponding author).

‡Professor, School of Energy Science and Engineering, 92 West Dazhi Street; libingx@hit.edu.cn.

m, m' = discrete-ordinates direction
MLS = moving least-squares approximation

I. Introduction

In the past decade, transient radiative transfer (TRT) in participating media has received considerable attention in many emerging applications. The recent developments in microscale systems [1], pulsed laser interaction with materials [2,3], optical tomography [4,5], laser therapy [6], and other applications have indicated that TRT is an important process that requires rigorous study. Many analytical studies and numerical models of TRT have been conducted. Brewster and Yamada [7] reported a computational and experimental investigation regarding the feasibility of determining optical properties of turbid media from picosecond time-resolved light scattering measurements in conjunction with diffusion theory predictions and Monte Carlo (MC) simulations. Guo et al. [8] simulated three-dimensional TRT for short pulse laser transport in-scattering and absorbing media by the MC method. The experimental results of 60 picosecond pulsed laser transmission in-scattering media were presented and compared with simulation. Good agreement between the MC simulation and experimental measurement was found. Gentile [9] presented a method for accelerating time-dependent implicit MC radiative transfer calculations by using a discretization of the diffusion equation to calculate probabilities that are used to advance particles in regions with small mean free paths. To reduce the computational time, Lu and Hsu [10] employed the reverse (backward) MC method to solve a one-dimensional TRT problem in participating media. Sakami et al. [11] developed a time-dependent discrete-ordinates method to analyze ultrashort light pulse propagation in a two-dimensional anisotropically scattering medium. Wu and coworkers [12–14] and Tan and Hsu [15,16] used a time-dependent integral equation (IE) formulation to develop transient radiative transfer modeling. Chai and coworkers [17–19] used the finite-volume method to calculate transient radiative transfer within a semitransparent media. Wu and Ou [20] employed a modified differential approximation and a hybrid of the $P_{1/3}$ approximation to solve a transient radiative transfer problem within a participating medium exposed to collimated irradiation.

Because the problem domain needs to be discretized into a mesh, these traditional methods, especially the finite-volume method and the finite element method, suffer from drawbacks such as tedious meshing and remeshing. The meshless method [21–24] has been proposed for the problem of computational mechanics in order to avoid the tedious meshing and remeshing. The meshless method is used to establish a system of algebraic equations for the whole problem domain without the use of a predefined mesh. Recently, meshless methods were introduced into the radiative heat transfer community. Liu [25,26] employed the meshless local Petrov–Galerkin (MLPG) method [23–25] to solve a steady multidimensional radiative transfer problem. Although the MLPG possesses several advantages, one of the major difficulties in the implementation of MLPG is the numerical integration.

Recently, Zhang et al. [27] proposed a least-squares collocation meshless (LSCM) method for computational mechanics problems. In the LSCM implementation, a moving least-squares (MLS) approximation [21–24] is employed for constructing the trial functions. In addition to the collocation points that are used to construct the trial functions, a number of auxiliary points are also added to form the total residuals of the problem. The least-squares technique is used to obtain the solution of the problem by minimizing the sum of the residuals for all collocation and auxiliary points. The LSCM does not require any mesh so that it is a truly meshless method, and the difficulties in obtaining exact numerical integration are avoided. Recently, Tan et al. [28] employed the LSCM approach to solve problems involving steady radiative and conductive heat transfer. The results show that the LSCM approach is efficient, accurate, and stable, and can be used for solving steady coupled radiative and conductive heat transfer problems in absorbing, emitting, and scattering media. In this paper, we extended the LSCM method based on the discrete-ordinates equation to solve a transient radiative transfer in semitransparent participating media. Three numerical examples are studied in order to illustrate the performance of this new solution method in solving transient radiative transfer problems.

II. Mathematical Formulation

A. Transient Radiative Transfer Equation

Consider radiative transfer in an enclosure filled with a semitransparent media. The discrete-ordinates equation of transient radiative transfer can be written as [17–19]

$$\frac{1}{c}\frac{\partial I^m}{\partial t} + \mu^m \frac{\partial I^m}{\partial x} + \eta^m \frac{\partial I^m}{\partial y} + \xi^m \frac{\partial I^m}{\partial z} + \left(\kappa_a + \kappa_s - \frac{\kappa_s}{4\pi}\Phi^{m,m} w^m\right) I^m = \kappa_a I_b + \frac{\kappa_s}{4\pi} \sum_{m'=1, m' \neq m}^{M} I^{m'} \Phi^{m',m} w^{m'} \tag{1}$$

with boundary conditions

$$I_w^m = \varepsilon_w I_{bw} + \frac{1-\varepsilon_w}{\pi} \sum_{\mathbf{n}_w \cdot \mathbf{s}_{m'} > 0} I_w^{m'} |\mathbf{n}_w \cdot \mathbf{s}_{m'}| w^{m'} \tag{2}$$

Using the fully implicit scheme to discretize the transient term, Eq. (1) can be rewritten as

$$\mu^m \frac{\partial I^m}{\partial x} + \eta^m \frac{\partial I^m}{\partial y} + \xi^m \frac{\partial I^m}{\partial z} + \left(\frac{1}{c\Delta t} + \kappa_a + \kappa_s - \frac{\kappa_s}{4\pi}\Phi^{m,m} w^m\right) I^m = \kappa_a I_b + \frac{\kappa_s}{4\pi} \sum_{m'=1, m' \neq m}^{M} I^{m'} \Phi^{m',m} w^{m'} + \frac{1}{c\Delta t}[I^m]^{\text{old}} \tag{3}$$

B. Moving Least-Squares (MLS) Approximation

In the least-square collocation implementation [27], the problem domain and its boundaries are discretized with N_{col} collocation points. In addition to these N_{col} points, another N_{aux} auxiliary point is also used in the problem domain. The collocation points are used to construct the approximate function $\tilde{I}^m(\mathbf{x})$ for the unknown radiative intensity $I^m(\mathbf{x})$ by the MLS approximation. Consider a spatial subdomain $V_{\mathbf{x}}$ in the neighborhood of a point $\mathbf{x}$ and denoted as the domain of definition for the MLS approximation of the trial function at $\mathbf{x}$, which is located within the problem domain. To approximate the distribution of the radiative intensity I^m in $V_{\mathbf{x}}$, over a number of local nodes $\{\mathbf{x}_i\}$, $i = 1, 2, \ldots, n$, the MLS approximant $\tilde{I}^m(\mathbf{x})$ of I^m, $\forall\ \mathbf{x} \in V_{\mathbf{x}}$, can be defined by [21–24]

$$\tilde{I}^m(\mathbf{x}) = \sum_{j=0}^{k} p_j(\mathbf{x}) a_j(\mathbf{x}) = \mathbf{p}^T(\mathbf{x})\mathbf{a}(\mathbf{x}) \tag{4}$$

where $\mathbf{p}^T(\mathbf{x}) = [p_1(\mathbf{x}), p_2(\mathbf{x}), \ldots, p_k(\mathbf{x})]$ is a complete monomial basis function of order k, and $\mathbf{a}(\mathbf{x})$ is a vector containing coefficients $a_j(\mathbf{x})$, $j = 1, 2, \ldots, k$, which are functions of the spatial coordinates $\mathbf{x} = [x, y, z]^T$. The coefficient vector $\mathbf{a}(\mathbf{x})$ is determined by minimizing a weighted discrete L_2 norm, defined as [21–24]

$$J[\mathbf{a}(\mathbf{x})] = \sum_{i=1}^{n} w_i^{\text{MLS}}[\mathbf{p}^T(\mathbf{x}_i)\mathbf{a}(\mathbf{x}) - \hat{I}_i^m]^2 \tag{5}$$

where $\mathbf{x}_i$ denotes the value of $\mathbf{x}$ at node i; $\hat{I}_i^m$ in Eq. (5) is the fictitious nodal intensity; $w_i^{\text{MLS}}(\mathbf{x})$ is the MLS weight function associated with node i, with $w_i^{\text{MLS}}(\mathbf{x}) > 0$ for all $\mathbf{x}$ in the support domain $V_{\mathbf{x}}$ of $w_i^{\text{MLS}}(\mathbf{x})$; and n is the number of nodes in $V_{\mathbf{x}}$ for which the weight functions $w_i^{\text{MLS}}(\mathbf{x}) > 0$. Here, $\hat{I}_i^m$ in Eq. (5) is a fictitious nodal value and not the nodal value, of the unknown trial function $\tilde{I}_i^m$ in general.

Minimization of J with respect to $\mathbf{a}(\mathbf{x})$ leads to the following linear relation between $\mathbf{a}(\mathbf{x})$ and $\hat{\mathbf{I}}^m$ [21–24]:

$$\mathbf{A}(\mathbf{x})\mathbf{a}(\mathbf{x}) = \mathbf{B}(\mathbf{x})\hat{\mathbf{I}}^m \tag{6}$$

where the matrices $\mathbf{A}(\mathbf{x})$, $\mathbf{B}(\mathbf{x})$ and $\hat{\mathbf{I}}^m$ are defined by [23–25]

$$\mathbf{A}(\mathbf{x}) = \sum_{i=1}^{n} w_i^{\mathrm{MLS}}(\mathbf{x})\mathbf{p}(\mathbf{x}_i)\mathbf{p}^T(\mathbf{x}_i) \tag{7}$$

$$\mathbf{B}(\mathbf{x}) = [w_1^{\mathrm{MLS}}(\mathbf{x})\mathbf{p}(\mathbf{x}_1), w_2^{\mathrm{MLS}}(\mathbf{x})\mathbf{p}(\mathbf{x}_2), \ldots, w_n^{\mathrm{MLS}}(\mathbf{x})\mathbf{p}(\mathbf{x}_n)] \tag{8}$$

$$\hat{\mathbf{I}}^m = [\hat{I}_1^m, \hat{I}_2^m, \ldots, \hat{I}_n^m] \tag{9}$$

Solving for $\mathbf{a}(\mathbf{x})$ from Eq. (6) and substituting it into Eq. (4) gives a relation which may be written in the form of an interpolation function as

$$\tilde{I}^m(\mathbf{x}) = \sum_{i=1}^{n} \phi_i(\mathbf{x})\hat{I}_i^m, \quad \forall\ \mathbf{x} \in V_{\mathbf{x}} \tag{10}$$

where

$$\phi_i(\mathbf{x}) = \sum_{j=1}^{k} p_j(\mathbf{x})[\mathbf{A}^{-1}(\mathbf{x})\mathbf{B}(\mathbf{x})]_{ji} \tag{11}$$

Here, $\phi_i(\mathbf{x})$ is the shape function of the ith node determined using the nodes that are included in the spatial subdomain $V_{\mathbf{x}}$ of $\mathbf{x}$ [21]. The partial derivatives of the shape function are obtained as [21–24]

$$\phi_{i,l}(\mathbf{x}) = \sum_{j=1}^{k}\{p_{j,l}[\mathbf{A}^{-1}\mathbf{B}]_{ji} + p_j[\mathbf{A}^{-1}\mathbf{B}_{,l} + (\mathbf{A}^{-1})_{,l}\mathbf{B}]_{ji}\} \tag{12}$$

where $(\,)_{,l} = \partial(\,)/\partial l$ represents the derivative with respect to spatial coordinate l, $l = x, y, z$.

C. Discretization and Numerical Implementation

Substituting Eqs. (10–12) into Eq. (3), we can obtain the following residual function R_Q^m for the discrete-ordinates equation defined in the problem domain

$$R_Q^m = \sum_{j=1}^{n} D^m[\phi_j(\mathbf{x}_Q)]I_j^m - C^m(\mathbf{x}_Q), \quad Q = 1, 2, \ldots, N_{\mathrm{col}} + N_{\mathrm{aux}} \tag{13}$$

where

$$D^m[\phi_j(\mathbf{x}_Q)] = \mu^m\phi_{j,x}(\mathbf{x}_Q) + \eta^m\phi_{j,y}(\mathbf{x}_Q) + \xi^m\phi_{j,z}(\mathbf{x}_Q) + \left(\frac{1}{c\Delta t} + \kappa_a + \kappa_s - \frac{\kappa_s}{4\pi}\Phi^{mm}w^m\right)\phi_j(\mathbf{x}_Q) \tag{14a}$$

$$C^m = \sum_{j=1}^{n}\phi_j(\mathbf{x}_Q)\left(\kappa_a I_b(\mathbf{x}_j) + \frac{\kappa_s}{4\pi}\sum_{m'=1,m'\neq m}^{M} I^{m'}(\mathbf{x}_j)\Phi^{m'm}w^{m'} + \frac{1}{c\Delta t}[I^m(\mathbf{x}_j)]^{\mathrm{old}}\right) \tag{14b}$$

Then, we obtain the following functional of all residuals for all collocation and auxiliary points

$$\Gamma = \sum_{Q=1}^{N_{\mathrm{col}}+N_{\mathrm{aux}}}\left\{\sum_{j=1}^{n} D^m[\phi_j(\mathbf{x}_Q)]I_j^m - C^m(\mathbf{x}_Q)\right\}^2 \tag{15}$$

Minimizing the functional Γ with respect to the radiative intensity I_i^m, we have

$$\frac{\partial\Gamma}{\partial I_i^m} = 2\sum_{Q=1}^{N_{\mathrm{col}}+N_{\mathrm{aux}}}\left\{\sum_{j=1}^{n} D^m[\phi_j(\mathbf{x}_Q)]I_j^m - C^m(\mathbf{x}_Q)\right\}D^m[\phi_i(\mathbf{x}_Q)] = 0, \quad i = 1, 2, \ldots, N_{\mathrm{col}} \tag{16}$$

This leads to the following discretized system of linear equations:

$$\sum_{j=1}^{N_{\mathrm{col}}} K_{ij}^m I_j^m = f_i^m, \qquad i = 1, 2, \ldots, N_{\mathrm{col}} \tag{17}$$

where

$$K_{ij}^m = \sum_{Q=1}^{N_{\mathrm{col}}+N_{\mathrm{aux}}} D^m[\phi_j(\mathbf{x}_Q)]D^m[\phi_i(\mathbf{x}_Q)] \tag{18a}$$

$$f_i^m = \sum_{Q=1}^{N_{\mathrm{col}}+N_{\mathrm{aux}}} C^m(\mathbf{x}_Q)D^m[\phi_i(\mathbf{x}_Q)] \tag{18b}$$

It is noted that the shape function and its derivatives are independent of the values of radiative intensity. Therefore, the iteration is linear. Equation (17) is solved independently for each direction, and the boundary conditions [Eq. (2)] must be imposed on the inflow boundary. For each node i on the inflow boundary, the radiative intensity I_i^m is given by Eq. (2), and the boundary condition can be directly imposed as follows:

$$K_{ij}^m = \begin{cases} 1 & i = j \\ 0 & i \neq j \end{cases} \tag{19a}$$

$$f_i^m = I_i^m \tag{19b}$$

Because the in-scattering term of the discrete-ordinates equation in direction m contains the radiative intensities of the other directions, global iterations similar to that used in the discrete-ordinates method are necessary in order to include the source and boundary conditions.

The implementation of the LSCM method for solving a transient radiative transfer problem can be carried out according to the following routine:

1) Choose a finite number of collocation points in the problem domain and its boundaries. Select the basis function and the MLS weight function.

2) Use the collocation points to construct the MLS approximation function $\tilde{I}^m(\mathbf{x})$ at all of the collocation and auxiliary points. Calculate shape function $\phi_i(\mathbf{x}_Q)$ and the first order derivatives.

3) Calculate the coefficients defined in Eqs. (18a) and (18b), and solve the linear system Eq. (17) to obtain the fictitious nodal values $\hat{I}^m$ for each discrete direction.

4) Terminate the iteration process if the specified stopping criterion is satisfied. Otherwise, go back to step 3.

5) Go back to step 3 to carry out the calculation for the next time step.

III. Results and Discussion

To verify the accuracy of the LSCM approach for solving transient radiative transfer problems in absorbing, emitting and scattering media, three particular test cases are examined. A computer code based on the preceding calculation procedure was written. Node densification and the dimensionless size parameter studies are also performed. For the following numerical study, the function of quartic spline with compact supports is used to construct the weight function for the MLS approximation

$$g(r) = \begin{cases} 1 + 6r^2 + 8r^3 - 3r^4, & r \leq 1 \\ 0, & r > 1 \end{cases} \tag{20}$$

For the sake of comparison, the relative error based on the data in references is defined as

$$\text{relative error} = 100 \times \frac{[\int_0^L (\text{data obtained by LSCM} - \text{data in references})^2 \, dx]^{1/2}}{\int_0^L \text{data in references} \, dx} \tag{21}$$

A. One-Dimensional Absorbing, Nonemitting, and Scattering Medium Between Parallel Black Plates

We consider a transient radiative transfer problem in an absorbing, nonemitting, and isotropically scattering medium bounded by two parallel black plates. The plates and the medium are initially at absolute zero (0 K). The thickness of the medium is L. At time $t = 0$, the temperature of the left boundary ($x/L = 0$) is suddenly raised to provide an emissive power of $\sigma T_{w_0}^4 = \pi$ for all subsequent time. The optical thickness $\tau_L = \beta L$ and the scattering albedo ω of medium are 1 and 0.5, respectively.

The LSCM approach is used to solve for the dimensionless incident radiation and radiative heat flux in the medium. $N_{\text{col}} = 21$ collocation points are uniformly distributed in the problem domain and on its boundaries. In addition, $N_{\text{aux}} = 20$ auxiliary points are also used in the problem domain. The equal weight even quadrature S_{12} is selected to discretize the angular space. The monomial basis function $\mathbf{p}^T(\mathbf{x}) = [1, x, x^2]$ is used, and the weight function for the MLS approximation is given as follows [21–27]:

$$w^{\text{MLS}}(\mathbf{x} - \mathbf{x}_i) = g\left(\left|\frac{x - x_i}{\alpha_{\text{MLS}} \Delta x}\right|\right) \tag{22}$$

where Δx is the average nodal spacing between two neighboring nodes and $\alpha_{\text{MLS}} = 2.5$ is used for the MLS approximation. For all computations in this case, the dimensionless time step is taken as $\Delta t^* = 0.005$.

The profiles of dimensionless incident radiation and radiative heat flux are shown in Figs. 1 and 2, respectively, and compared with the exact values obtained by Tan and Hsu [15] using the IE method. The LSCM results agree with the data obtained by Tan and Hsu [15] very well. The maximum relative error of the dimensionless incident radiation and the dimensionless radiative heat flux are less than 4.1 and 5.3%, respectively.

The effects of the dimensionless time step are shown in Figs. 3 and 4. It can be seen that, by decreasing the time step, the LSCM results are closer to the exact values obtained by Tan and Hsu, but more computational time will be consumed. Even with the dimensionless time step of $\Delta t^* = 0.01$, the comparison is quite good.

B. Two-Dimensional Absorbing and Emitting Medium in Irregular Quadrilateral Enclosure

As shown in Fig. 5, we consider an irregular quadrilateral enclosure (all dimensions are in meters). The enclosure is filled with an absorbing and emitting medium. The absorption coefficient is taken to be 1 m^{-1}. The medium and black enclosure walls are initially kept at 0 K. At time $t = 0$, the medium is suddenly increased to a constant temperature of T_g.

The LSCM approach is used to solve for the transient evolution of radiative heat fluxes on the bottom wall. As shown in Fig. 5, $N_{\text{col}} = 256$ collocation points are distributed in the problem domain and on its boundaries. In this case, no auxiliary points are used. The equal weight even quadrature S_8 is selected to discretize the angular space. The monomial basis function $\mathbf{p}^T(\mathbf{x}) = [1, x, y, x^2, xy, y^2]$ is used, and

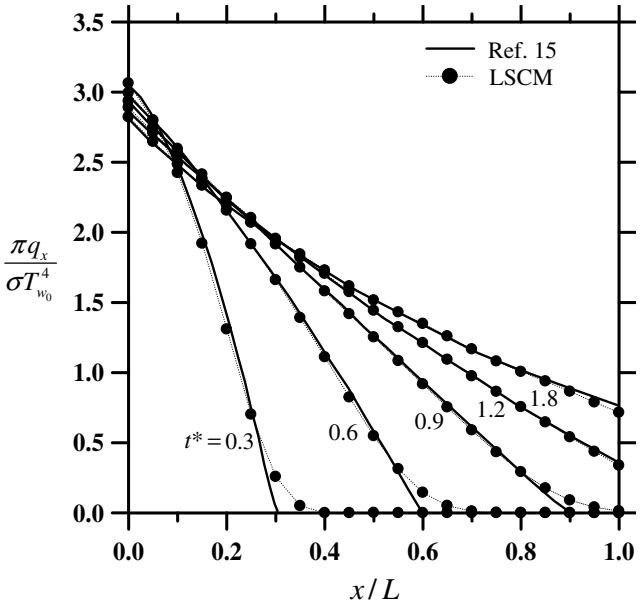

Fig. 2 Dimensionless radiative heat flux distributions at different dimensionless times.

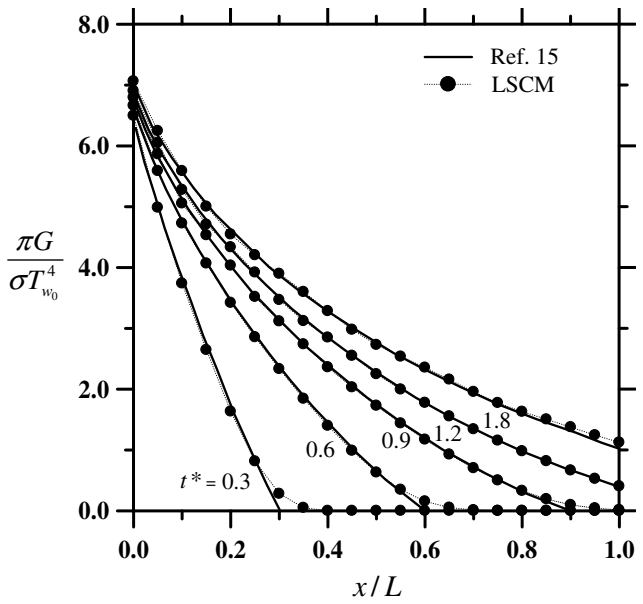

Fig. 1 Dimensionless incident radiation distributions at different dimensionless times.

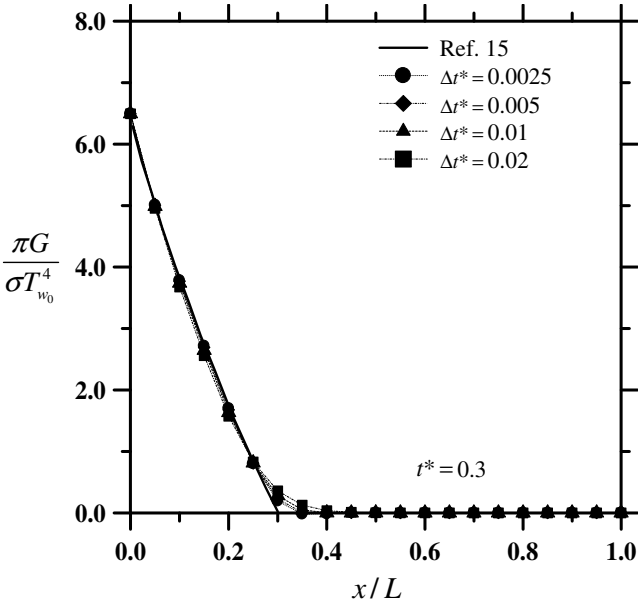

Fig. 3 Effect of dimensionless time step on the solution accuracy for incident radiation.

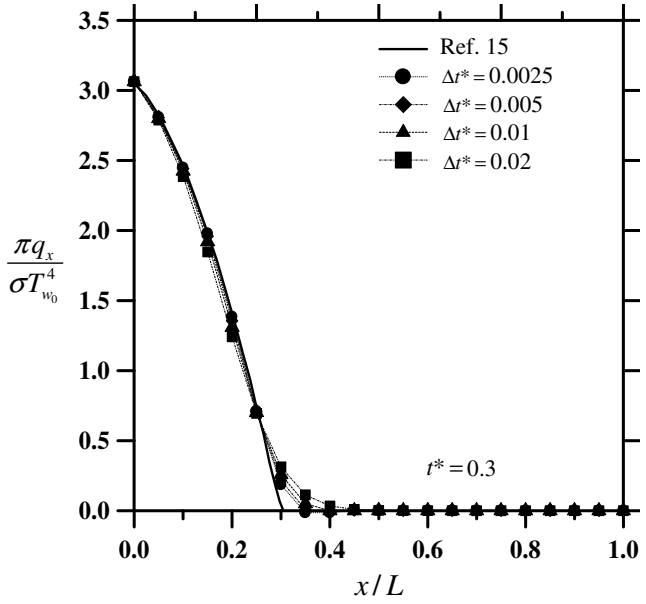

Fig. 4 Effect of dimensionless time step on the solution accuracy for radiative heat flux.

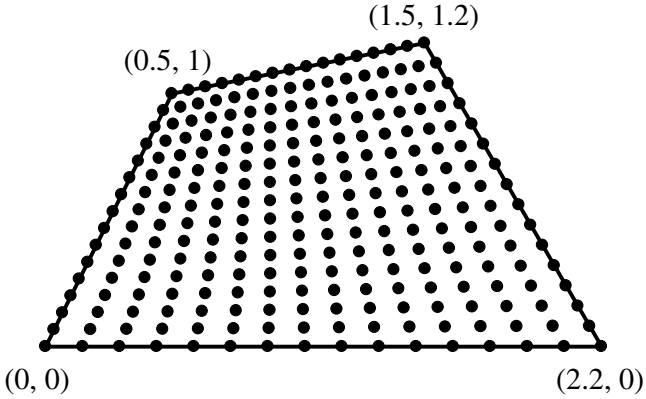

Fig. 5 Schematic and node system of an irregular quadrilateral enclosure (dimensions in meters).

the weight function for the MLS approximation is given as follows [21–27]:

$$w^{\mathrm{MLS}}(\mathrm{x}-\mathrm{x}_i) = g\left(\left|\frac{x-x_i}{\alpha_{\mathrm{MLS}}\Delta x}\right|\right) g\left(\left|\frac{y-y_i}{\alpha_{\mathrm{MLS}}\Delta y}\right|\right) \qquad (23)$$

where Δx and Δy are the average nodal spacings between two neighboring nodes in the x and y coordinate directions, respectively, and $\alpha_{\mathrm{MLS}} = 2.5$ is used for the MLS approximation. For all computations in this case, the dimensionless time step is taken as $\Delta t^* = 0.025$.

The dimensionless radiative heat fluxes on the bottom wall at four different dimensionless times are shown in Fig. 6, and compared with the solution obtained by Chai [18] using the finite-volume method. The LSCM results agree with the data obtained by Chai [18] very well. The maximum relative error is less than 1.4%.

To check the convergence of the LSCM, we use three different collocation point numbers, namely, 121, 256, and 441, to discretize the problem domain, and solve for the dimensionless radiative heat fluxes on the bottom wall at dimensionless time $t^* = 0.25$. The effect of the number of collocation points is shown in Fig. 7. It can be seen that, by increasing the number of collocation points, the LSCM results are closer to the solution obtained by Chai [18]. The relative errors are 2.3, 1.41, and 1.40% for the cases of $N_{\mathrm{col}} = 121$, $N_{\mathrm{col}} = 256$, and $N_{\mathrm{col}} = 441$, respectively. As viewed from the relative errors, there is no major difference between the results

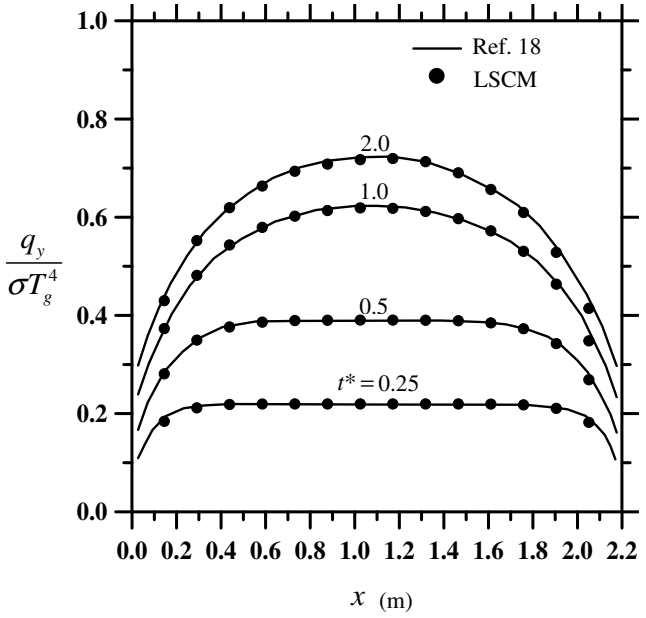

Fig. 6 Transient evolution of radiative heat fluxes on the bottom wall.

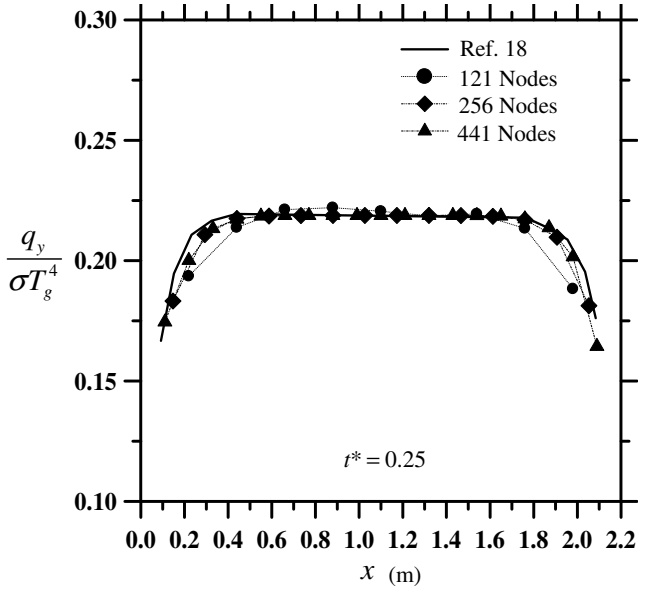

Fig. 7 Effect of collocation point number on solution accuracy for radiative heat fluxes on the bottom wall.

obtained using 256 and 441 collocation points. This means that the essential physics of the model is independent of node number for this case when $N_{\mathrm{col}} \geq 256$. As shown in Fig. 7, even with 121 collocation points (N_{col}), the comparison is quite good. The convergence of the LSCM is demonstrated in Fig. 7.

α_{MLS} is an important parameter which determines the number of collocation points in the definition domain of the MLS approximation for the trial functions. To check the effect of α_{MLS}, we use four different α_{MLS}, namely, 2.1, 2.5, 3.0, and 3.5, to construct the MLS approximation for the trial functions, and solve for the dimensionless radiative heat fluxes on the bottom wall at the dimensionless time $t^* = 0.25$. Figure 8 shows the effect of α_{MLS}. If the order of the monomial basis function is $k = 6$, there are 6 undetermined coefficients $a_j(\mathbf{x})$, $j = 1, 2, \ldots, 6$, in the MLS approximation of $\tilde{I}^m(\mathbf{x})$ [see Eq. (4)]. Therefore, the number of collocation points n in the definition domain of the MLS approximation must not be less than 6. To ensure the required number of points, α_{MLS} must be larger than 2.0. As shown in Fig. 8, when α_{MLS} is larger than 3.0, the numerical results will oscillate. This suggests that in order to obtain a

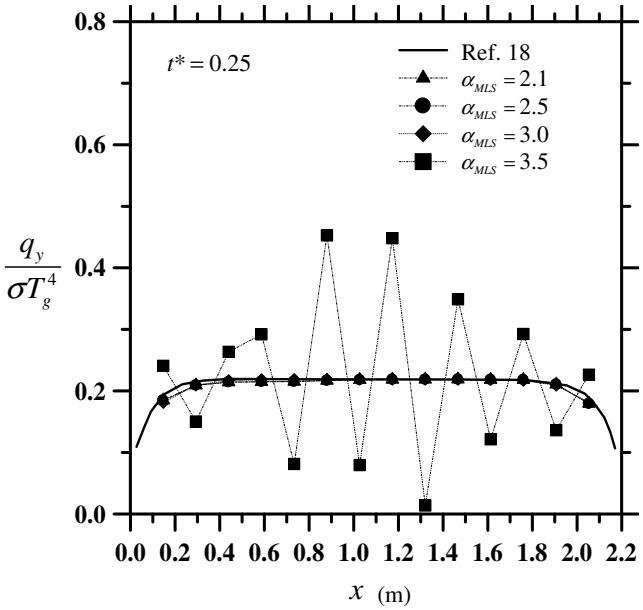

Fig. 8 Effect of α_{MLS} on the stability of solution.

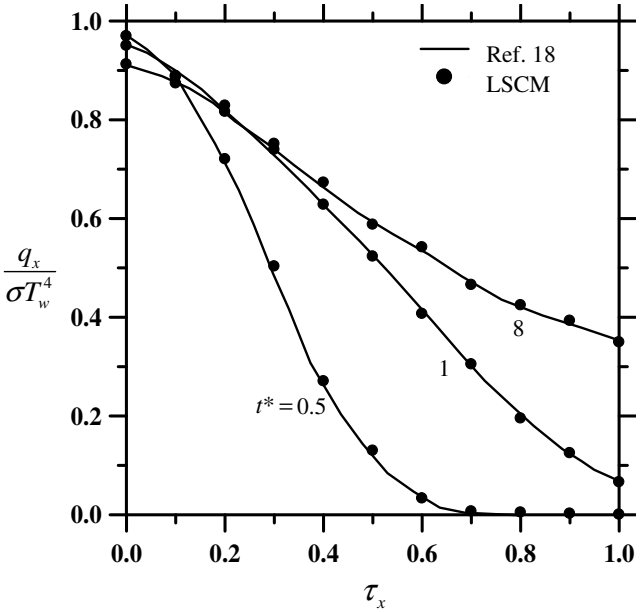

Fig. 10 Dimensionless radiative heat flux profiles along the symmetry line at $\tau_y = 0.5$.

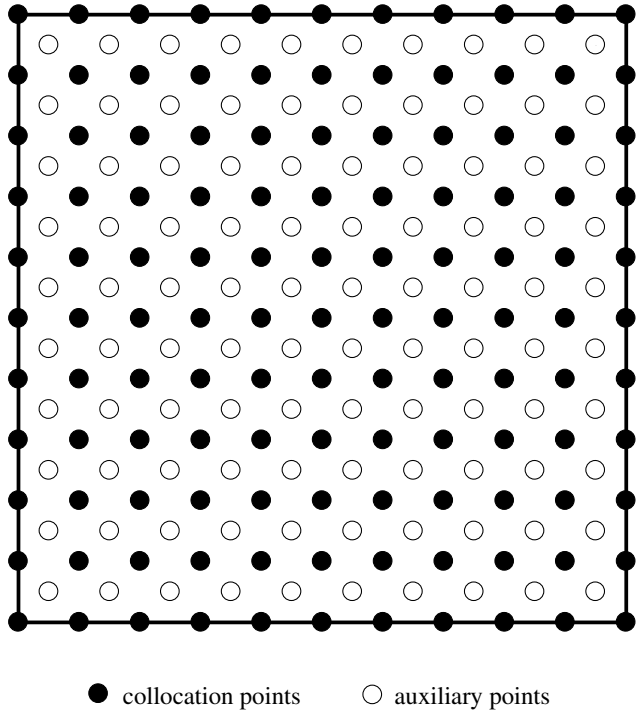

Fig. 9 Schematic and node system of the rectangular enclosure.

stable solution in this case, the dimensionless size parameter should be within the region between 2.0 and 3.0.

C. Two-Dimensional Anisotropically Scattering Medium in a Square Enclosure

In this case, as shown in Fig. 9, we study a transient radiative transfer problem in a square enclosure filled with an absorbing and anisotropically scattering medium. The boundary walls are black and initially at absolute zero (0 K). At time $t = 0$, the temperature of the left boundary ($x = 0$) is suddenly increased to provide an emissive power of σT_w^4 for all subsequent time. The scattering albedo and the optical thickness based on the side length of the square enclosure are both set to 1.0. The medium scatters radiation anisotropically according to the F2 phase function reported in Kim and Lee [29]:

$$\Phi = \sum_{j=0}^{8} C_j P_j(\mu) \tag{24}$$

where P_j is the Legendre polynomial. The C_j are the expansion coefficients defined as $C_0 = 1.0$, $C_1 = 2.00917$, $C_2 = 1.56339$, $C_3 = 0.67407$, $C_4 = 0.22215$, $C_5 = 0.04725$, $C_6 = 0.00671$, $C_7 = 0.00068$, $C_8 = 0.00005$. The quadrature scheme of the discrete-ordinates equation, the monomial basis function, and the weight function for the MLS approximation are same as those given in case B. The selection of monomial basis function and weight function can be seen in Wu and Ou [22] in detail.

The LSCM approach is used to solve for the transient evolution of radiative heat fluxes on the bottom wall. As shown in Fig. 9, $N_{\mathrm{col}} = 121$ collocation points are uniformly distributed in the problem domain and on its boundaries. In addition, $N_{\mathrm{aux}} = 100$ auxiliary points are also used in the problem domain. The dimensionless time step is taken as $\Delta t^* = 0.05$, and the dimensionless size parameter is chosen as $\alpha_{\mathrm{MLS}} = 2.5$. The radiative heat fluxes along the symmetry line at $\tau_y = 0.5$ are shown in Fig. 10 for three different dimensionless times, namely, $t^* = 0.5$, $t^* = 1.0$, and $t^* = 8.0$, respectively, and are compared with the solution obtained by Chai [18] using the finite volume method. The maximum relative error of the LSCM results is 3.7%. The LSCM approach has good accuracy to solve this purely scattering transient radiative transfer problem.

IV. Conclusion

A least-squares collocation meshless method based on the discrete-ordinates equation is extended to solve transient radiative transfer problems in absorbing, emitting, and scattering media. The fully implicit scheme is used to discretize the transient term. A moving least-squares approximation is applied to construct the trial functions. The least-squares technique is used to obtain the solution of the problem by minimizing the sum of the residuals for all collocation and auxiliary points. Three numerical results are compared with the other benchmark approximate solutions. By comparison, the results show that least-squares collocation meshless method is efficient, accurate and stable, and can be used for solving transient radiative transfer problems in participating media. For two-dimensional problems, if the order of monomial basis is six, the dimensionless size parameter should be within the region of 2.0 to 3.0, and 2.5 appears to be the best choice to obtain a stable solution.

Acknowledgment

The support of this work by the National Nature Science Foundation of China (50425619, 50576018) is gratefully acknowledged.

References

[1] Tien, C. L., Majumdar, A., and Gerner, F., *Microscale Energy Transport*, Begell House, New York, 1998, pp. 1–93.

[2] Longtin, J. P., and Tien, C. L., "Saturable Absorption During High Intensity Laser Heating of Liquids," *Journal of Heat Transfer*, Vol. 118, No. 4, 1996, pp. 924–930.

[3] Qiu, T. Q., and Tien, C. L., "Short Pulse Laser Heating in Metals," *International Journal of Heat and Mass Transfer*, Vol. 35, No. 3, 1992, pp. 719–726.

[4] Yamada, Y., and Tien, C. L., "Light-Tissue Interaction and Optical Imaging in Biomedicine," *Annual Review of Fluid Mechanics and Heat Transfer*, Vol. 6, Begell House, New York, 1995, pp. 1–59.

[5] Liu, F., Yoo, K. M., and Alfano, R. R., "Ultrafast Laser-Pulse Transmission and Imaging Through Biological Tissues," *Applied Optics*, Vol. 32, No. 4, 1993, pp. 554–558.

[6] Grant, M. J. C., and Welch, A. J., "Clinical Use of Laser-Tissue Interaction," *IEEE Engineering in Medicine and Biology Magazine*, Vol. 8, No. 4, 1989, pp. 10–13.

[7] Brewster, M. Q., and Yamada, Y., "Optical Properties of Thick, Turbid Media from Picosecond Time-Resolved Light Scattering Measurements," *International Journal of Heat and Mass Transfer*, Vol. 38, No. 14, 1995, pp. 2569–2581.

[8] Guo, Z. X., Aber, J., Garetz, B. A., and Kumar, S., "Monte Carlo Simulation and Experiments of Pulsed Radiative Transfer," *Journal of Quantitative Spectroscopy and Radiative Transfer*, Vol. 73, Nos. 2–5, 2002, pp. 159–168.

[9] Gentile, N. G., "Implicit Monte Carlo Diffusion: An Acceleration Method for Monte Carlo Time-Dependent Radiative Transfer Simulations," *Journal of Computational Physics*, Vol. 172, No. 2, 2001, pp. 543–571.

[10] Lu, X. D., and Hsu, P. F., "Reverse Monte Carlo Method for Transient Radiative Transfer in Participating Media," *Journal of Heat Transfer*, Vol. 126, No. 4, 2004, pp. 621–627.

[11] Sakami, M., Mitra, K., and Hsu, P. F., "Analysis of Light Pulse Transport through Two-Dimensional Scattering and Absorbing Media," *Journal of Quantitative Spectroscopy and Radiative Transfer*, Vol. 73, No. 2–5, 2002, pp. 169–179.

[12] Wu, Y., and Wu, S. H., "Integral Equation Formulation for Transient Radiative Transfer in an Anisotropically Scattering Medium," *International Journal of Heat and Mass Transfer*, Vol. 43, No. 11, 2000, pp. 2009–2020.

[13] Wu, C. Y., "Propagation of Scattered Radiation in a Participating Planar Medium with Pulse Irradiation," *Journal of Quantitative Spectroscopy and Radiative Transfer*, Vol. 64, No. 5, 2000, pp. 537–548.

[14] Wu, S. H., and Wu, C. Y., "Time-Resolved Spatial Distribution of Scattered Radiative Energy in a Two-Dimensional Cylindrical Medium with a Large Mean Free Path for Scattering," *International Journal of Heat and Mass Transfer*, Vol. 44, No. 14, 2001, pp. 2611–2619.

[15] Tan, Z. M., and Hsu, P. F., "An Integral Formulation of Transient Radiative Transfer," *Journal of Heat Transfer*, Vol. 123, No. 3, 2001, pp. 466–475.

[16] Tan, Z. M., Hsu, P. F., and Chai, J. C., "Transient Radiative Transfer in Three-Dimensional Homogeneous and Non-Homogeneous Participating Media," *Journal of Quantitative Spectroscopy and Radiative Transfer*, Vol. 73, No. 2–5, 2002, pp. 181–194.

[17] Chai, J. C., "One-Dimensional Transient Radiation Heat Transfer Modeling Using a Finite-Volume Method," *Numerical Heat Transfer, Part B, Fundamentals*, Vol. 44, No. 2, 2003, pp. 187–208.

[18] Chai, J. C., "Transient Radiative Transfer Modeling in Irregular Two-Dimensional Geometries," *Journal of Quantitative Spectroscopy and Radiative Transfer*, Vol. 84, No. 3, 2004, pp. 281–294.

[19] Chai, J. C., Hsu, P. F., and Lam, Y. C., "Three-Dimensional Transient Radiative Transfer Modeling Using the Finite-Volume Method," *Journal of Quantitative Spectroscopy and Radiative Transfer*, Vol. 86, No. 3, 2004, pp. 299–313.

[20] Wu, Y., and Ou, N. R., "Differential Approximations for Transient Radiative Transfer Through a Participating Medium Exposed to Collimated Irradiation," *Journal of Quantitative Spectroscopy and Radiative Transfer*, Vol. 73, No. 1, 2002, pp. 111–120.

[21] Liu, G. R., *Mesh Free Methods*, CRC Press, Boca Raton, FL, 2003, pp. 67–248.

[22] Liu, G. R., and Gu, Y. T., *An Introduction to Meshfree Methods and Their Programming*, Springer, New York, 2005, pp. 54–144.

[23] Zhang, X., and Liu, Y., *Meshless Methods*, Tsinghua University Press, Beijing, 2004, pp. 144–176.

[24] Atluri, S. N., and Shen, S. P., *The Meshless Local PPetrov–Galerkin (MLPG) Method*, Tech Science Press, Encino, CA, 2002, pp. 93–214.

[25] Liu, L. H., "Meshless Local PPetrov–Galerkin Method for Solving Radiative Transfer Equation," *Journal of Thermophysics and Heat Transfer*, Vol. 20, No. 1, 2006, pp. 150–154.

[26] Liu, L. H., "Meshless Method for Radiative Heat Transfer in Graded Index Medium," *International Journal of Heat and Mass Transfer*, Vol. 49, No. 1–2, 2006, pp. 219–29.

[27] Zhang, X., Liu, X. H., Song, K. Z., and Lu, M. W., "Least-Squares Collocation Meshless Method," *International Journal for Numerical Methods in Engineering*, Vol. 51, No. 9, 2001, pp. 1089–1100.

[28] Tan, J. Y., Liu, L. H., and Li, B. X., "Least-Squares Collocation Meshless Approach for Coupled Radiative and Conductive Heat Transfer," *Numerical Heat Transfer, Part B, Fundamentals*, Vol. 49, No. 2, 2006, pp. 179–195.

[29] Kim, T. K., and Lee, H. S., "Effect of Anisotropic Scattering on Radiative Transfer in Two-Dimensional Rectangular Enclosures," *International Journal of Heat and Mass Transfer*, Vol. 31, No. 8, 1988, pp. 1711–1721.